Polymer Shelled Microparticles for a Targeted Doxorubicin Delivery in Cancer Therapy

ARTICLE *in* BIOMACROMOLECULES · MARCH 2011

Impact Factor: 5.75 · DOI: 10.1021/bm101207k · Source: PubMed

Biomacromolecules

ARTICLE

pubs.acs.org/Biomac

Polymer Shelled Microparticles for a Targeted Doxorubicin Delivery in Cancer Therapy

Barbara Cerroni, Ester Chiessi, Silvia Margheritelli, Letizia Oddo, and Gaio Paradossi*

Dipartimento di Scienze e Tecnologie Chimiche, University of Rome Tor Vergata, Via della Ricerca Scientifica, 00133 Rome, Italy

Supporting Information

ABSTRACT: Targeting is a main feature supporting any controlled drug delivery modality. Recently we developed poly(vinyl alcohol), PVA, based microbubbles as a potential new ultrasound contrast agent featuring an efficient ultrasound backscattering and a good shelf stability. The chemical versatility of the polymeric surface of this device offers a vast variety of coupling modalities useful for coating and specific targeting. We have designed a conjugation strategy on PVA shelled microbubbles to enable the localization and the drug delivery on tumor cells by modifying the surface of this polymeric ultrasound contrast agent (UCA) with oxidized hyaluronic acid (HAox). After the conversion of the microbubbles into microcapsules, the kinetics of the release of doxorubicin, a well-known antitumor drug, from uncoated and HAox-coated PVA microbubbles and microcapsules was investigated. Cytocompatibility and bioadhesive properties of the HA-modified microparticles were then tested on the HT-29 tumor cell line. Cytotoxicity to HT-29 tumor cells of microcapsules after loading with doxorubicin was studied, evidencing the efficacy of the HAox coating for the delivery of the drug to cells. These features are a prerequisite for a theranostic, that is, diagnostic and therapeutic, use of polymer-based UCAs.

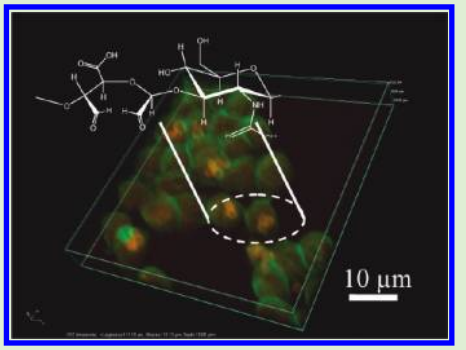

1. INTRODUCTION

The formulation of new devices to be used as contrast agents with enhanced diagnosis and therapeutic functionalities is a key subject in nanomedicine. Next-generation of contrast agents for medical imaging will also support localized drug delivery functions based on the biointerface between the micro/nano ultrasound contrast agent (UCA) and the tissue to monitor and treat. This scenario requires an integrated approach concerning the targeting[1,2] and the specificity of the UCA surface coating by using biomolecules with recognized ability for pharmacological signal transduction. This strategy, recently reviewed,[3] has been applied to marketed lipid-based microbubbles that have been decorated with antibodies (anti-VEGF and anti-ICAM),[4−7] RGD[8] and heterodimeric peptides[9] for the molecular targeting of tumor angiogenesis factors, biodhesion regulating molecules, integrins, and kinase insert domain receptor, respectively.

Hyaluronic acid, HA,[10] owns a well-documented recognition for cell receptor proteins falling into three main groups: CD44 (Cluster Determinant 44),[11,12] RHAMM (Receptor for HA Mediated Motility),[13] and ICAM-1 (Intercellular Adhesion Molecule-1). CD44 and ICAM-1 were already known as cell adhesion molecules with other recognized ligands before their HA binding was discovered.[14] Cell−matrix interactions mediated by the CD44/HA receptor−ligand pair are involved in the regulation of leukocyte migration and activation.[15−17] Moreover, CD44 has been reported in the literature as a marker or indicator of several cancer types (prostate, ovarian, breast) and it is expressed at high levels in colon cancer cells.[18−21] In this respect, HA is a natural candidate to implement UCA surface for a specific targeting of tumor cells.

Recently we have developed a UCA with enhanced properties with respect to commercially available ultrasound contrast agents.[22,23] The system is made of microbubbles (MBs) with a poly(vinyl alcohol), PVA, based shell and an air-filled core.[24] PVA[25] is a polymer already used in biomedicine as material for stents,[26] stitches, and more in general as bioinert support material. Functionalized PVA chains bearing reactive aldehydes as terminal groups are cross-linked to the hydroxyl groups present in the PVA repeating units via an acetalization reaction carried out at the water/air interface created by foaming the PVA aqueous solution. Within 2 h, the foam is converted into a stable suspension of microbubbles with a shell formed by cross-linked PVA chains floating on top of the aqueous medium. The stability of PVA-based microbubbles, having an average diameter of 2−3 μm with a narrow distribution, extends over many months in water.[24,27,28] A table summarizing the main structural features of this system and a schematic representation of MB shell are reported in Part 1 of the Supporting Information. These air-filled core particles offer assets as a good chemical versatility of the shell, promoting tethering and coating of the microbubble particle with suitable ligands, a good ultrasound backscattering efficiency,[29] and drug and gas loading enhanced efficiency.[30]

Received: October 11, 2010
Revised: December 20, 2010
Published: January 14, 2011

All these features allow the consideration of microbubbles as a concept for a next-generation ultrasound contrast agent with enhanced functionalities toward a device supporting imaging and enabling localized drug release for a dual, diagnostic and therapeutic, approach. In this paper we address the issue of the coating of the microbubbles with a special focus on the surface functionalization with HA. Hyaluronic acid belongs to the class of glycosaminoglycans with a glucuronic acid and an *N*-acetylglucosamine linked together by a $\beta[1\rightarrow3]$ glycosidic linkage forming the disaccharide repeating unit. The equatorial position of the C2 and C3 hydroxyl groups of the glucuronic residue is keen to be selectively oxidized by metaperiodate. The oxidation causes the opening of the saccharide ring with two aldehyde functionalities exploitable for conjugating HA on the microbubble surface.

The main aim of this work is to design a strategy leading to the conjugation of the polymer surface of the outlined new microbubbles with hyaluronic acid for the targeting of tumor cells and tissues. Evaluation of the interaction with human adenocarcinoma cells is discussed to establish a relationship between structural parameters characterizing the microbubbles coating and surface interactions with cells. The loading and the release process of doxorubicin, a well-known antitumor drug, and the delivery of this drug to human adenocarcinoma cells were also studied.

2. EXPERIMENTAL SECTION

2.1. Materials. Poly(vinyl alcohol) (PVA) was a Sigma product. Number average molecular weight of PVA, determined by membrane osmometry, was 30000 ± 5000 g/mol, and weight average molecular weight, determined by static light scattering, was 70000 ± 10000 g/mol.

Sodium hyaluronate (HA), with a number average molecular weight of 700000 g/mol, was a kind gift from Fidia Farmaceutici, Abano (PD), Italy.

Sodium (meta)periodate ($NaIO_4$) with purity grade ≥99.0%, *tert*-butyl carbazate (TBC) with purity grade of 98%, sodium cyanoborohydride ($NaBH_3CN$) reagent grade, deuterium oxide (D_2O) with a deuteration degree of 99.9%, containing 0.05% (w/w) of 3-(trimethylsiliyl)propionic-2,2,3,3-d_4 acid (TMS) sodium salt and benzoylated dialysis tubing with average flat width of 32 mm and molecular weight cut off, MWCO, of 2000 g/mol were Sigma (Milan, Italy) products.

Doxorubicin hydrochloride (DOXO) with purity ≥98.0%, fluorescein isothiocyanate isomer I (FITC) and rhodamine B isothiocynate (TRITC) were purchased from Fluka (Milan, Italy).

Ethylene glycol (analytical grade), sodium hydroxide as anhydrous pellets with 98% purity, sodium chloride (analytical grade), methanol with 99.9% purity, sodium acetate (analytical grade), acetic acid, and hydrochloric acid 37% (w/v) were purchased from Carlo Erba (Milan, Italy). Water was Milli-Q purity grade (18.2 MΩ·cm), produced with a deionization apparatus (PureLab) from USF. Dialysis membranes with a MWCO of 12000−14000 Da were purchased from Medicell, Italy. Dialysis membranes with a cut-off of 3500 Da were a Pierce, U.S.A., product. Human adenocarcinoma cell line, HT-29, was purchased from Istituto Zooprofilattico Sperimentale della Lombardia e dell'Emilia Romagna, Brescia, Italy. McCoy's 5A medium, fetal bovine serum (FBS), L-glutamine, penicillin, and streptomycin were purchased from Euroclone (Milan, Italy). Trypsin 10X solution was purchased from Lonza (Basel, Switzerland). Phosphate buffered saline (PBS), pH 7.4, phalloidin-FITC, thiazolyl blue tetrazolium bromide (MTT) were from Sigma-Aldrich (Milan, Italy). Triton X-100 and formaldehyde were purchased from Fluka (Milan, Italy). Dimethyl sulfoxide (DMSO) and inorganic salts were from Carlo Erba (Milan, Italy).

Table 1. Reaction Conditions of HA Oxidation

$GlcUA/IO_4^-$ molar ratio	reaction time (h)	
$GlcUA/IO_4^-$ = 1:0.1	3	HAox0.1
$GlcUA/IO_4^-$ = 1:0.2	84	HAox0.2
$GlcUA/IO_4^-$ = 1:0.8	84	HAox0.8
$GlcUA/IO_4^-$ = 1:3	84	HAox1

2.2. Methods. *2.2.1. Synthesis of PVA Microbubbles.* Stable (air-filled) PVA microbubbles were prepared by cross-linking telechelic PVA, that is, PVA bearing aldehydes as chain terminals, at the water/air interface.[24] Briefly, 4 g of PVA were added in 200 mL of Milli-Q water. The suspension was stirred at 80 °C until complete PVA dissolution. A total of 0.380 g of sodium (meta)periodate was added to the solution and the reaction was carried out at 80 °C for 1 h with constant stirring. After cooling the solution to room temperature, the microbubbles were formed by stirring vigorously the solution with an Ultra-Turrax T-25 at 8000 rpm equipped with a Teflon-coated tip at room temperature for 2 h.

Floating microbubbles were separated from solid debris, extensively washed in separatory funnels, and stored in Milli-Q water for further use.

2.2.2. HA Oxidation. The oxidation reaction of hyaluronic acid was carried out in aqueous solution with different molar quantities of $NaIO_4$, as reported in Table 1. GlcUA is the glucuronic acid residue present in the HA repeating unit.

The reaction was kept in the dark and stopped by adding ethylene glycol. The polymer solution was purified by dialysis against 0.2 M NaCl for 1 day and then extensively dialyzed using dialysis tubes with MWCO of 2000 Da against water. Oxidized HA samples were stored as a freeze-dried powder. The scheme of the chemical structure of the HAox samples is reported in Part 2 of the Supporting Information.

Determination of the degree of oxidation in the periodate-oxidized HA (HAox) was carried out by a Bruker 300 MHz ^{1}H NMR, coupling *tert*-butyl carbazate (TBC) to the HAox samples containing aldehydes. HAox was dissolved in 0.1 M acetate buffer (pH = 5.2) at a concentration of 10 mg/mL. TBC, dissolved in the same buffer, was added up to a 5-fold molar excess over GlcUA residues of HA. $NaBH_3CN$ in 1:1 molar ratio with TBC was then added to the oxidized hyaluronic acid solutions for reductive amination coupling. This reaction was carried out also on native HA as control.

The reaction mixture was allowed to react for 24 h. The polymer was dialyzed against 0.1 M NaCl solution, and then extensively against Milli-Q quality water and stored as a freeze-dried powder. The freeze-dried product was investigated by ^{1}H NMR and the aldehyde and acetyl contents were assessed by comparing the signals at 1.4 ppm (9H, carbazate t-Boc) and 2.0 ppm (3H, HAox acetamide),[31] respectively, taking as reference the TMS signal.

The degree of oxidation was evaluated also by monitoring the consumption of periodate during the reaction according to the change in the absorbance at 220 nm with the UV−vis spectrophotometer Jasco V-630, Japan. When comparing the data determined by the two methods, the contributions of IO_3^- ion and of oxidized hyaluronic acid absorbance at 220 nm are taken into account in the UV determinations of the degree of oxidation.

2.2.3. Circular Dichroism of Oxidized Hyaluronic Acid Aqueous Solutions. The spectra were recorded in the range 200−250 nm using a Jasco J600 spectropolarimeter with Hellma (GE) quartz cells with an optical path of 1 mm. The concentrations of HAox0.1, HAox0.2, HAox0.8, and HAox1 solutions were always equal to 2 mg/mL.

2.2.4. Synthesis of Microbubbles Coated with Hyaluronic Acid (HAox-MBs). Hyaluronic acid samples with different degrees of oxidation, HAox0.1, HAox0.2, HAox0.8 and HAox1, were coupled with the microbubbles surface by acetalization. A scheme of the junction between HA and PVA chains is reported in Part 3 of the Supporting Information. Typically, freeze-dried HAox samples were solubilized in Milli-Q water

to a concentration of 5 mg/mL. A suspension of microbubbles (1 mg MBs/10 mg HAox) was added to the solution and the pH was adjusted to 3.0. The reaction proceeded for 24 h, then the suspension of conjugated microbubbles with HAox was extensively washed in separatory funnels and stored in Milli-Q water. Elemental analysis on sample HAox0.2-MBs resulted in a hyaluronic content over the MBs total mass of 0.45% (w/w).

2.2.5. Synthesis of FITC-Labeled Oxidized Hyaluronic Acid. Decoration of microbubbles with HAox at different degrees of oxidation was confirmed by tagging HAox with FITC. In this way microbubbles surface is detectable by fluorescence microscopy or by confocal laser scanning microscopy (CLSM), using an Ar^+ ion laser (excitation wavelength 488 nm) due to the presence of fluorescently labeled polymer molecules conjugated on the microbubble shell.

FITC at a concentration of 2 mg/mL in methanol was added into 1% (w/v) oxidized polymer solutions in Milli-Q water. In the resulting solution, the weight ratio between FITC and oxidized polymer was 0.1/g oxidized polymer. After 3 h of reaction in the dark at room temperature, the FITC-labeled polymers were precipitated with ethanol to extract the unreacted FITC and redissolved in water for dialysis against deionized water (dialysis membrane with MWCO of 2000) and freeze-dried. The FITC-labeled polymers were used for the synthesis of HA coated microbubbles to study by CLSM. Description of the experimental set up used for CLSM imaging is reported in section 2.2.10.

2.2.6. Transformation of Air-Filled Microbubbles into Buffer-Filled Microcapsules (MCs) and Fluorescent Labeling. Microbubbles (5 mL of suspension at a concentration of 1 mg/mL) were placed into 10 mL of an ethanol/water 70% (v/v) solution. After equilibrating for three days, microbubbles were converted into MCs, which sediment at the bottom of the test tube. Microcapsules were then extensively washed.

MCs fluorescent labeling was accomplished as follows: a sample of MCs (1 mg/mL) was reacted with 2 μL of TRITC 2.5 mM in agitation for 1 h and then washed repeatedly until colorless washings. A sterilization process was further carried out by exposing the microcapsules in a Petri dish for 30 min under a UV lamp (100 W).

The main structural features of microcapsules are described in the paper of Paradossi et al.[24]

2.2.7. Drug Release Study of Targeted Microbubbles and Microcapsules. The drug loading of the microbubbles was performed by equilibrating the MBs in a dispersion medium containing a DOXO concentration of 0.09 mg/mL for 5 days. The amount of DOXO loaded onto microbubbles was determined by measuring the absorption at 480 nm of the drug solution used for charging the microbubbles before and after the loading. An average cargo of 0.5 ± 0.1% (w/w) was assessed for the HAox1 coated MBs, corresponding to $(3.0 \pm 0.6) \times 10^{-5}$ ng of DOXO/microbubble. An average cargo of $(1.0 \pm 0.3) \times 10^{-5}$ ng of DOXO/microbubble was obtained for the uncoated MBs. The DOXO release study was carried out on HAox1 coated and uncoated MBs. After loading with DOXO and washing in separatory funnel, the microbubbles were placed in a PBS buffer solution (3 mL) in a dialysis bag having a MWCO of 3500 Da surrounded by 15 mL of PBS solution. The whole system was placed in a thermostatic bath at 37 °C. Absorbance of the surrounding solution (the dialysate) at 480 nm was recorded as a function of the time. Blank experiments were carried out to measure the time constant of the diffusion process of doxorubicin in the absence of microbubbles.

The DOXO loading and the release study of the microcapsules were performed according to the procedure used for microbubbles. A DOXO average cargo of $(1.4 \pm 0.3) \times 10^{-4}$ ng of DOXO/microcapsule and of $(1.4 \pm 0.7) \times 10^{-4}$ ng of DOXO/microcapsule was obtained for uncoated and HAox1-coated MCs, respectively.

2.2.8. ζ-Potential Measurements. ζ-Potential measurements were carried out on HAox1-coated and uncoated MBs at 25 °C with a particle analyzer NanoZetaSizer (Malvern Instruments LTD, U.K.). A total of 1.0 mL of particle dispersion in Milli-Q grade water at a concentration of 10 mg/mL was loaded in the measuring cell. Results were the average of six repetitions.

2.2.9. Cell Culturing. HT-29 (human colon adenocarcinoma cells) from Istituto Zooprofilattico Sperimentale della Lombardia e dell'Emilia Romagna, Brescia (Italy), were cultured in McCoy's 5A medium, supplemented with 10% FBS, 20 mM of L-glutamine, 100 U/mL penicillin, and 100 μg/mL streptomycin at 37 °C in a 5% CO_2 atmosphere.

2.2.10. Viability Tests (MTT Assay). In the present investigation, HT-29 cells, counted with a Neubauer chamber, were seeded in 24-well plates to allow the attachment onto the surface of the wells for 12 h. Then the cells were treated with different kinds and amounts of microcapsules. MTT, dissolved in PBS solution (5 mg/mL), was added at fixed times in the wells up to a concentration of 10% of the total culture volume to form formazan purple crystals as reaction product with cellular mitochondrial metabolites.[32] After 4 h, the solution over the crystals was removed and replaced with DMSO, a good solvent for the water-insoluble formazan. Plates were further incubated for 5 min at room temperature and the absorbance at 570 nm was recorded by UV spectroscopy (Jasco V-630, Japan).

2.2.11. Cell Staining. Cells were stained using phalloidin-FITC, which provides a green fluorescent labeling of the cytoskeleton due to its specific binding with F-actin. Phalloidin-FITC was solubilized in DMSO to form a stock solution with a concentration of 0.1 mg/mL.

Cells, grown on sterile coverslips, were rinsed twice with PBS buffer solution and then fixed for 10 min in 3.7% formaldehyde in PBS. After washing with PBS, permeabilization with 0.1% Triton-X 100 in PBS for 7 min was carried out. The specimen, washed with PBS, was stained using a 50 μg/mL fluorescent phalloidin-FITC solution in PBS. After 40 min at room temperature, cells were rinsed with PBS twice and samples were observed with the confocal laser scanning microscope Nikon Eclipse Ti-E with 100× or 60× oil immersion objectives.

FITC and TRITC fluorescence stainings were detected exciting the sample at 488 and 543 nm with Ar^+ (Melles Griot) and He−Ne (Spectra Physics) lasers, respectively. Images capture and processing were carried out using EZ-C1 and NIS software packages (Nikon).

3. RESULTS AND DISCUSSION

Polymer shelled microbubbles can represent a new type of ultrasound contrast agent with interesting features as narrow size polydispersity, great shelf stability, and good ultrasound backscattering.[33,34]

Moreover, microbubbles offer a good chemical versatility with a robust cross-linked polymeric shell where conjugation of ligand molecules and drugs can be attempted, even though any conjugation on the surface of this device requires mild reaction conditions as aqueous media, room temperature, and non toxic reagents. The number of coupling options are further restricted by the chemical features of the ligand responsible for the device targeting. Focusing on HA as ligand molecule, a possible strategy for its coupling onto the MBs surface is an interfacial acetalization reaction, involving the hydroxyl groups of the PVA surface. A similar strategy, used on the collagen-rich aortic valve leaflets for improving the coating of different prosthetic devices as heart valves and stents, focuses on the partial modification of glycosaminoglycans, the polysaccharides' family where HA is included, to allow chemical cross-linking of this important class of biopolymers to the device surface for a more robust, long lasting coating with improved biointerfacial features.[35,36]

The aldehydes introduced on the polysaccharide backbone are required for the conjugation on the MBs surface via an acetalization coupling. This can be easily achieved by specific oxidation of HA by metaperiodate, a reaction requiring the equatorial arrangement

Table 2. Determination of the Oxidation Degree of HA and HAox Samples by ^{1}H-NMR and UV Spectroscopies[a]

	oxidation degree by UV (%)	oxidation degree by ^{1}H NMR (%)
HA		3
HAox0.1	1	2
HAox0.2	15	8
HAox0.8	60	48
HAox1	97	91

[a] Errors within 10%.

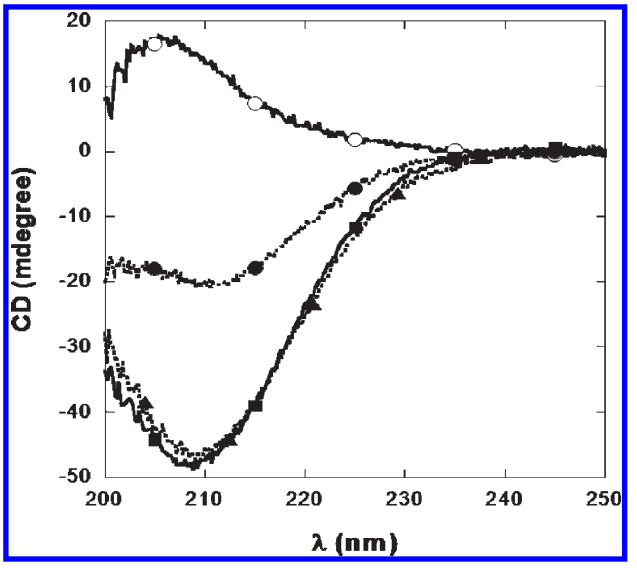

Figure 1. CD spectra of HA (-■-), HAox0.2 (-▲-), HAox0.8 (-●-), and HAox1 (-○-): optical path, 1 mm; polymer concentration, 2 mg/mL.

of the C2 - C3 hydroxyl groups of the glucuronic acid residue of the HA repeating unit. As the reaction proceeds slowly, the tuning of the amount of oxidized repeating units can be easily achieved by quenching the reaction with a molar excess of ethylene glycol. We have oxidized HA to different extents to determine the optimal conditions, enabling the conjugation with hydroxyl groups on the microbubbles surface and to estimate the targeting efficiency on adenocarcinoma cells.

The oxidation degree of HA was determined by ^{1}H NMR, using *tert*-butyl carbazate (TBC)[31,37] to quantify the presence of aldehyde groups in the HA repeating units. Integrals of acetyl group peak resonance at 2.0 ppm of the acetyl glucosamine residue of the HA repeating unit and of the *t*-butyl group peak at 1.46 ppm were used to obtain the acetylation and oxidation degrees, respectively, after the periodate splitting reaction taking as external reference the TMS peak area. The ^{1}H NMR spectrum of the oxidized hyaluronic acid HAox0.8 with TBC is reported in Part 4 of the Supporting Information. The NMR analysis was compared with the results obtained by UV absorption at 220 nm by monitoring the IO_4^- ions consumption due to the reaction progressing.[38] In Table 2, the results obtained with both methods are summarized.

Circular dichroism (CD) spectra (see Figure 1) of aqueous solutions of oxidized hyaluronic acid and of HA show that the oxidation extent of HA backbone influences the ellipticity of the band at 208 nm.[39] Interestingly, for HAox1, an inversion of the sign of the ellipticity at 208 nm was observed. The change of the

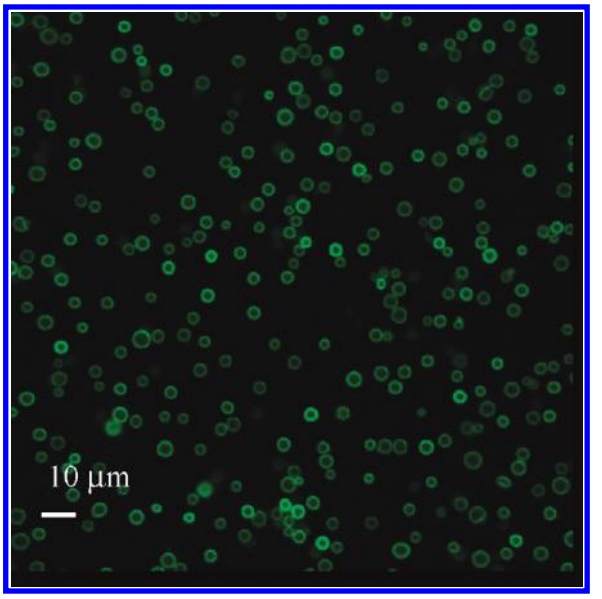

Figure 2. CLSM image of FITC-labeled HAox1-coated microbubbles.

specific optical rotation (ORD) at the D line of sodium alginate and of the corresponding periodate-oxidized polymer was investigated by Painter et al.[38] The sign inversion, from negative to positive, was due to the formation of hemiacetals with nearest neighbor residues to the oxidized glucuronic saccharide unit of alginate backbone. In our case, hemiacetal formation can occur as well, accompanied by a change in the ellipticity of the $n \rightarrow \pi^*$ electronic transition when passing from native HA to HAox samples with increasing degree of oxidation. This is consistent with the general rules governing the relationship between ORD and CD.[40]

HA coating on MBs surface, accomplished by condensation in mild conditions of HA oxidized at different extents with PVA shell, was validated by laser scanning confocal microscopy. Oxidized HA samples were fluorescently labeled by FITC coupling prior to the conjugation with MBs. CLSM images of MBs showed (see Figure 2) the typical ring shapes representing the equatorial plane of the focused microbubbles.

3.1. Doxorubicin Release by PVA Microbubbles and Microcapsules. To assess how the coating influences the release of drug from the device surface, we studied the in vitro release behavior of HA-coated microbubbles after loading with doxorubicin, an anticancer drug whose spectroscopic features allow an easy monitoring of the drug released. Release from uncoated and HAox1-coated microbubbles was examined.

The microbubbles were loaded with DOXO by equilibrating them for 5 days in a PBS buffer solution containing doxorubicin at 0.09 mg/mL. After washing, the dispersion of microbubbles (3 mL) was placed in a dialysis bag surrounded by 15 mL of the same buffer. Absorbance of the external solution, the dialysate, at 480 nm was recorded as a function of time. Blank experiments were carried out to measure the time constant of the diffusion process of DOXO in the absence of microbubbles. The spectroscopic determination of the release of the drug directly on the dispersing medium of the MBs was not possible due to residual scattering caused by the presence of the microbubbles in the buffer.

Data were examined treating the release mechanism as two consecutive first order processes considering only the data in the initial stage. The first step is the DOXO detachment from the

Table 3. Doxorubicin Release Characteristic Times at 37 °C

	blank	uncoated microbubbles	HAox1-coated microbubbles	uncoated microcapsules	HAox1-coated microcapsules
τ_{obs} (h)		1.7 ± 0.2	7.7 ± 0.6	2.7 ± 0.5	2.8 ± 0.5
τ_1 (h)		≪1.7	∼7.7		
τ_2(h)	1.7 ± 0.1				

microbubbles shells, with time constant τ_1, and the second step is represented by the diffusion of the drug through the dialysis membrane, with time constant τ_2.

Within these assumptions, the time dependence of the UV absorption, Abs(t), at 480 nm of the dialysate is given by

$$\mathrm{Abs}(t) = \mathrm{Abs}_\infty\left[1 - \frac{1}{1-(\tau_2/\tau_1)}\cdot\exp(-t/\tau_1) + \frac{1}{(\tau_1/\tau_2)-1}\cdot\exp(-t/\tau_2)\right] \quad (1)$$

where Abs_∞ is the absorbance value at infinite time.

Equation 1 becomes a monoexponential function if one of the two steps is rate-determining:

$$\mathrm{Abs}(t) = \mathrm{Abs}_\infty[1-\exp(-t/\tau_{obs})] \quad (2)$$

with a time constant τ_{obs} corresponding to τ_1 or τ_2, depending on whether the doxorubicin diffusion from the microbubble shells or the diffusion of doxorubicin through the dialysis membrane is the rate determining process. By carrying out the same experiment in the absence of microbubbles, that is, in the condition where the only process is the diffusion of DOXO molecules through the dialysis membrane, the characteristic time of diffusion through the dialysis membrane, τ_2, is determined.

The time behavior of Abs(t) for the release of doxorubicin is described by eq 2 both for the uncoated and for the HAox1-coated microbubbles and the time constants of the release processes are summarized in Table 3.

The τ_{obs} value obtained for the release from the uncoated microbubbles is equal to the characteristic time of the diffusion process from the dialysis bag, τ_2, a result indicating that the detachment of DOXO from the uncoated microbubble shells occurs in a very short time, that is, $\tau_1 \ll \tau_2$. In the case of the HAox1-coated microbubbles, the release of doxorubicin is modulated by the particle coating, with a release time constant τ_{obs} about 5-fold larger than τ_2. We attribute the difference in τ_{obs} of the uncoated and coated MBs as an indication of electrostatic interaction of the positively charged DOXO molecules with the negative charges of the HA coating, slowing down the release process from the HAox1-coated microbubbles. This hypothesis has been validated by the measurement of the ζ-potential of uncoated and HA-coated microbubbles, providing the values of -2.9 ± 0.3 and -18 ± 1 meV, respectively. It is worthwhile to note that the characteristic time for the detachment of DOXO from HAox1-coated microbubble shells should enable the adhesion of the MBs with cells before the drug release process takes place.

The in vitro release of DOXO from buffer-filled microcapsules, directly derived from the microbubbles, was studied with the same method used for the release by MBs. Within the first 24 h, about 15% of the drug cargo was released by MCs. In this initial stage, the time behavior of the absorption at 480 nm of the dialysate showed a monoexponential increase for both uncoated and HAox1-coated microcapsules. By fitting the data according to eq 2 a τ_{obs} value, similar between uncoated and HAox1-coated MCs, was obtained (see Table 3). After the first 24 h, a slow linear increase of absorption with time was observed, indicating a zero order kinetic behavior. A deeper penetration of the loaded drug inside the microparticles' shell in the case of MCs, in comparison with MBs, can explain the higher average DOXO cargo of MCs, about 5-fold higher than that of MBs, and the similar average DOXO cargo of uncoated and HAox1-coated MCs. The results of this study by MCs indicate a biphasic modality of release, with a first phase not controlled by the microparticle coating, with a characteristic time lower than that observed for HAox1-coated MBs. The second phase of the release is a zero-order process, covering a few days. As for the HAox1-coated MBs, the release features of HAox1-coated microcapsules allow the interaction and adhesion of the microparticles with cells before the DOXO release occurs. A figure showing the DOXO release by HAox1-coated and uncoated MCs is reported in Part 5 of the Supporting Information.

3.2. PVA-Based Microcapsules Interaction with Cells. To have a background knowledge on features of the biointerface of PVA microbubbles, we addressed preliminarily the study of interaction with cells using buffer-filled microcapsules, MCs, directly derived from the microbubbles. The aim of this investigation was to test the efficiency of the coating for targeting tumor cells avoiding the buoyancy of the microbubbles to hinder the contact with the cell layer. In this section we describe the study of the interaction of MCs covalently coated with hyaluronic acid (HA) at different degrees of oxidation with HT-29 cell line (human colon adenocarcinoma), in which the transmembrane protein CD44 is overexpressed. HA is a polysaccharide found in the extracellular matrix and contributes, among other functions, to cellular adhesion and recognition of the receptor CD44. Our strategy was the coating of microbubbles shells with HA, followed by their transformation into buffer-filled microcapsules. The first step in the study of the interaction with cells was to assess the cytocompatibility of the MCs. HT-29 (50000 cells) viability was monitored by MTT assay after 3 days in the presence of different amounts of HAox0.1-coated microcapsules. The results of this experiment are reported in Figure 3, where a minor decrease in cell viability, about 15%, was observed when cells were incubated with the largest amount of MCs, corresponding to 320 MCs/cell.

A total of 50 and 100 μg of HAox0.1-coated microcapsules were incubated with 200000 cells, corresponding to 40 and 80 MCs/cell, respectively, for a cytocompatibility test over a period of 18 h. In Figure 4 the results obtained according to the MTT test are reported. A decrease of approximately one-third of the cellular metabolic activity was observed after 18 h by exposing 200000 HT-29 cells to 100 μg of the HAox0.1-coated MCs.

In another experiment, the cytocompatibility test was extended by exposing 50000 HT-29 cells to 100 μg of HAox1-coated microcapsules for 7 days, corresponding to 320 MCs/cell. The results, summarized in the bar graph of Figure 5, indicate about a one-third decrease in cellular viability for the longest exposures (6 and 7 days).

The interaction between microcapsules and cells was monitored to find a clear correlation with the extent of HA coating.

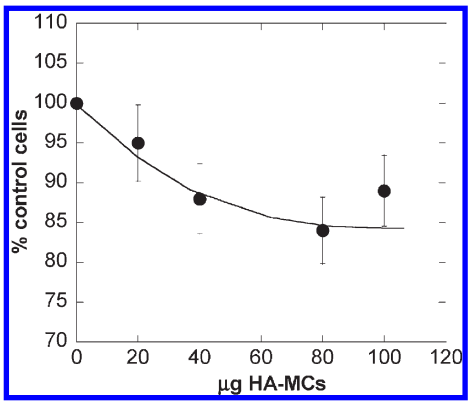

Figure 3. Viability (MTT assay) of 50000 HT-29 cells after incubation for 3 days with HAox0.1-coated microcapsules. Data represent mean values (±S.D.) of three independent experiments.

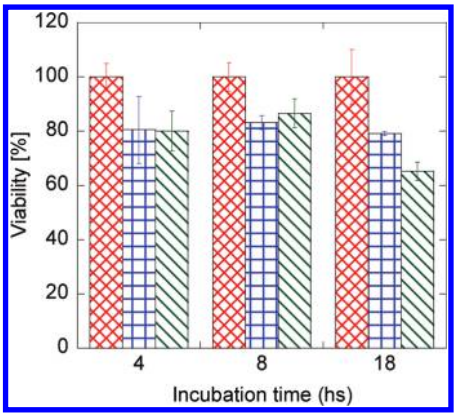

Figure 4. MTT assay at different incubation times (4, 8, and 18 h) on 200000 HT-29 cells exposed to different amounts of HAox0.1-coated microcapsules: metabolic activity of HT-29 cells in the absence of microcapsules (red bars); metabolic activity in the presence of 50 μg of HAox0.1-coated microcapsules, 40 MCs/cell, (blue bars); in the presence of 100 μg of HAox0.1-coated microcapsules, 80 MCs/cell (green bars). Data represent mean values (±S.D.) of three independent experiments.

To this aim, MCs were labeled with the fluorescent dye TRITC and cells were stained using phalloidin-FITC, detected in the red and green CLSM channels, respectively. We exposed HT-29 tumor cells to microcapsules coated with differently oxidized HA, observing at different times the effect of the surface coating on cellular internalization. In Figure 6, some of the bioadhered microcapsules coated with HAox1, pointed by the arrows, are visibly deformed by HT-29 cells.

In a former paper[30] we studied the shell elasticity of the microcapsules used in this work deforming them by osmotic stress. Sodium poly(styrene sulfonate) fractions at known concentration and molecular weight were used to establish an osmotic pressure build up between the liquid core of the microcapsule permeable only to diffusible species and the external dispersing medium, thus, promoting the buckling of the shells, as observed by CLSM microscopy.[30] Based on the observation of sets of 200 microcapsules, with this approach we determined that an osmotic stress of 1 MPa was required to buckle 50% of the microcapsules.

The flexibility of the MB shells is higher according to atomic force microscopy shell characterization.[41] From "Force−deformation"

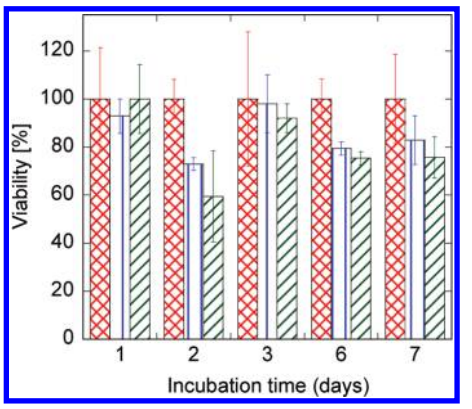

Figure 5. MTT test on the viability of 50000 HT-29 cells (control, red bar); in the presence of 100 μg of microcapsules (blue bar) and of 100 μg HAox1-coated microcapsules (green bar). Data represent mean values (±S.D.) of three independent experiments.

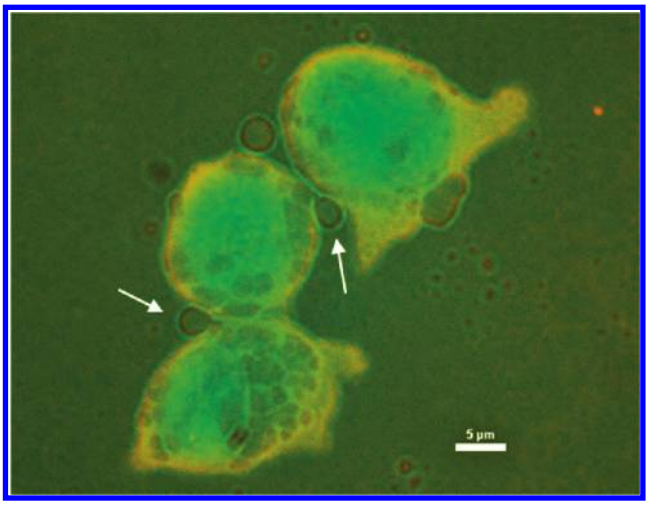

Figure 6. Fluorescence microscopy image of HAox1-coated microcapsules after incubation with HT-29 cells of 5 days. Deformed microcapsules are indicated by the arrows.

experiments on a single bubble, a pressure of 0.1 MPa can be evaluated for the deformation of microbubble shell, 1 order of magnitude smaller than for MCs.

Fibroblasts focal adhesions on a deformable elastomeric support were reported to promote a stress of 5.5 nN/μm.[2,42] The adhesion stress exerted by fibroblasts corresponds to about one tenth of the critical buckling pressure of microcapsules. This can be plausibly considered the pressure required for initiate the shell deformation.

The effects of incubation for 7 days of HT-29 cells with uncoated, HAox0.8- and HAox1- coated microcapsules were monitored by CLSM. To evidence only the specific interaction of MCs with HT-29, ruling out any physical association, extensive washings of the coverslips were carried out to wash out all scarcely adhered microcapsules. Representative CLSM images were captured, see Figure 7, showing that the number of microcapsules interacting with cells increases with the oxidation degree of the HA coating. It is noteworthy that the bioadhesion ability of the microcapsules is not hindered by the presence of the negatively charged uronic moiety, contrasting any aspecific association process with the negatively charged cellular membrane.

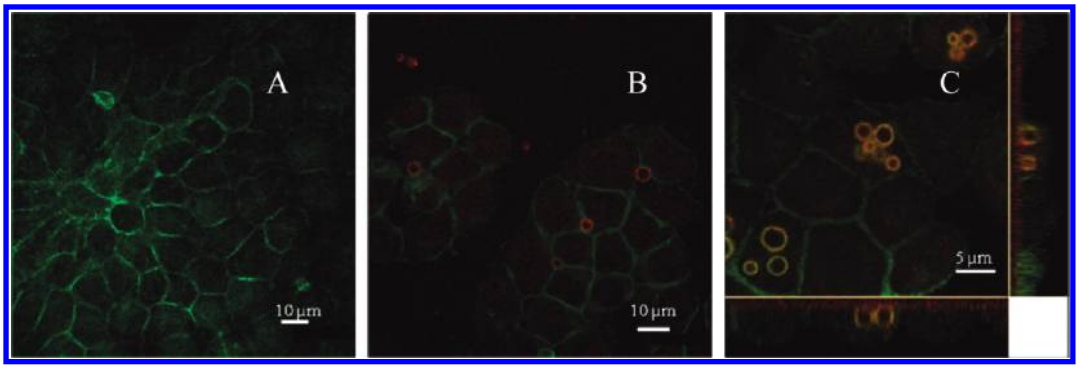

Figure 7. Interaction of HT-29 cells with microcapsules (red) after incubation for 7 days. CLSM images (*x*,*y* planes) of cells stained with FITC phalloidin (green) incubated with uncoated microcapsules: (A) with HAox0.8-coated microcapsules, and (B) with HAox1-coated microcapsules, (C) with *z*,*y* and *z*,*x* planes.

Table 4. Influence of HA Coatings on the Internalization Process by HT-29 Cells

uncoated microcapsules			HAox0.8-coated microcapsules			HAox1-coated microcapsules		
MC included	No. cells	No. MC/cell	No. MC included	No. cells	No. MC/cell	No. MC included	No. cells	No. MC/cell
0	50	0	3	16	0.20	12	40	0.3
1	45	0	5	51	0.10	7	23	0.3
						15	34	0.4
						10	25	0.4
						11	38	0.3
avg (±S.D.) No. of MCs/cell: 0 ± 0.05			avg (±S.D.) No. of MCs/cell: 0.15 ± 0.05			avg (±S.D.) No. of MCs/cell: 0.34 ± 0.03		

Interestingly, HT-29 cells are able to internalize HA-coated MCs, although in less extent if compared with macrophages.[43] In Figure 7C, the view of the orthogonal planes with respect to the $x-y$ plane evidence the position of the HAox1-coated MCs in the cytoplasm of the cells. However, the cytoplasm district involved in the uptake process as well as the mechanism need a deeper investigation. Spontaneous uptake of micrometer-sized particles by nonphagic cells[44] has been recently addressed to assess the effective potential of delivery and sensing functionalities of layer-by-layer microcapsules.[45−51] Cell lines differing in the proliferation behaviors and morphologies have been shown to incorporate polyelectrolyte microcapsules, although invariably the number of cells with internalized microcapsules were lower than the number of cells with externally adherent ones. Also, in the present study, the number of internalized microcapsules is remarkably lower than the microcapsules externally attached to the cells.

HT-29 cells endocytosis of microcapsules, in terms of the numbers of MCs internalized per cell, visualized by confocal microscopy, are summarized in Table 4 on separate batch experiments.

Endocytosis is enhanced by the presence of the HA coating characterized by a higher degree of oxidation. The amplification in the internalization process may be attributed to the larger amount of conjugated HA of the microcapsule coating. This result is noteworthy as it opens to the possibility of transferring the drug inside the targeted cell, with a major increase in the bioavailability and in the efficacy of the therapeutic treatment. We expect an enhanced internalization of PVA-shelled microbubbles with an HA coating due to the higher compliance of the shell.

3.3. Doxorubicin Delivery by PVA Microcapsules. As hyaluronic acid determines the favorable conditions for the microcapsules interactions with cells and regulates the release time window of doxorubicin, we tested the in vitro delivery properties of HAox1-coated microcapsules in the presence of HT-29 cells as well as the related cytotoxic effect of this drug, taking advantage of its easy detection in confocal microscopy due to the emission fluorescence of DOXO at 550−650 nm. Doxorubicin delivery has been supported by nanostructured devices as poly-γ-glutamic acid/doxorubicin complexes,[52] mesoporous silica nanoparticles coated by lipid bilayers,[53] and multifunctional polymeric micelles.[54] Lipoplexes have been extensively used for cell transfection in vitro and are also promising candidates for in vivo gene therapy.[55−57]

In our case, HAox1 coating results the most effective as far as the localization is concerned and the DOXO release is more prolonged with this coating. For these reasons, HT-29 cells were incubated in the presence of 100 μg of HAox1 MCs containing a DOXO cargo of about 0.5% (w/w). The drug release and accumulation in the cell nuclei is evident from the CLSM images taken after 24 h of incubation (Figure 8). The presence of DOXO is revealed by the red fluorescence staining of the nuclei, whereas the cell cytoplasm is characterized by the green fluorescence due to the phalloidin-FITC.

The number of HT-29 cells after prolonged incubation (5 days) with HAox1 coated MCs was very low, as most of the cells were easily detached during the washing and transfer of the coverslip processes, indicating qualitatively the cytotoxic effect of the drug released by the DOXO loaded MCs. For a more quantitative monitoring of the cytotoxic activity of the drug, we carried out a viability test (MTT assay) on 50000 HT-29 cells with 100 μg of HAox1-coated MCs, corresponding to 320 MCs/cell, without DOXO and with a payload of drug equal to 0.5 μg (Figure 9). For comparative purposes, we also assessed the effect of the exposure to free DOXO at a concentration of 1.7 μM,

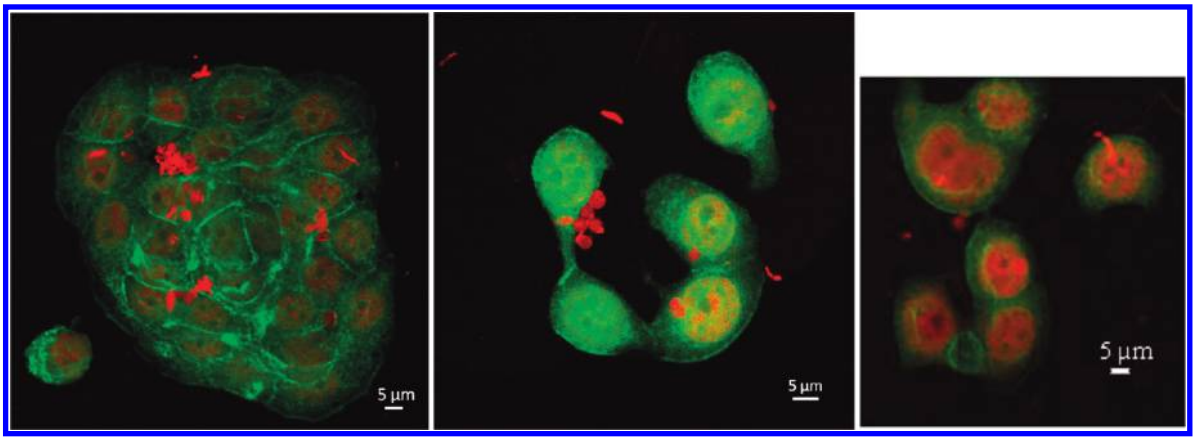

Figure 8. HT-29 cells after 24 h incubation with HAox1 MCs loaded with DOXO.

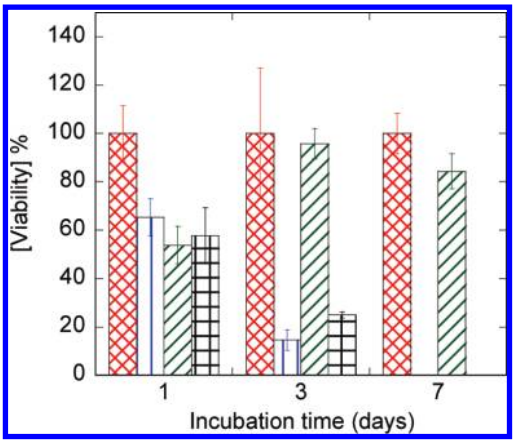

Figure 9. Cytotoxicity study of the DOXO released by HAox1-coated MCs up to 7 days: red bars, control; blue bars, free DOXO; green bars, in the presence of 100 μg of HAox1-coated microcapsules without DOXO; black bars, in the presence of 100 μg of HAox1-coated microcapsules loaded with DOXO. Data represent mean values (±S.D.) of three independent experiments.

corresponding to the highest concentration of DOXO in culture medium deliverable by the drug-loaded microcapsules.

The impact of the unloaded MCs on the cell viability is negligible through the whole experiment duration. On the contrary, the effect of DOXO within the first 3 days is cytostatic and the toxicity of the DOXO loaded MCs is comparable to that of free DOXO. The complete apoptosis of the cells after 7 days was observed. Overall, these results confirm the possibility to use HA coated microcapsules and microbubbles for the delivery of doxorubicin and indicate that the drug loaded onto microparticles fully retains its anticancer activity.

4. CONCLUSION

Poly(vinyl alcohol)-based microbubbles have been tested concerning features, as ultrasound behavior, structural analysis and biocompatibility.[24,28−30,33,34] In this work, we investigated the bioadhesion features of an ad hoc surface modification consisting of a coating with oxidized hyaluronic acid, a ligand for the CD44 receptor expressed in human tumor cells.

Specific oxidation of hyaluronic acid is required for a more efficient coating of the microbubbles and higher degrees of oxidation enhance the adhesion to the membrane of HT-29 tumor cells. Gas-core filled microbubbles were transformed into liquid-filled microcapsules, leaving unchanged the characteristics of the surface exposed to the dispersing medium. In this way, we could assess that periodate-oxidized HA represents an efficient coating for next generation ultrasound contrast agent, enabling the targeting and the bioadhesion. In this in vitro study, HA-based coating has a key role in promoting the MCs internalization. Despite the presence of the uronic moiety contrasting any aspecific association process with the negatively charged cellular membrane, adhesion to HT-29 cells is triggered with a cohesive action that enables the deformation of the shells and, in some cases, their internalization in the cytoplasmic compartments. The time requested for this uptake process is a few days and work to better assess such behavior is in progress. The localization of the microcapsules promotes the focal release of doxorubicin and enhances the drug bioavailability. To better exploit the MCs encapsulating process, we are designing a microbubble surface modification involving the covalent link of DOXO molecules to MBs, easily hydrolyzable by proteolytic enzymes present in the cell cytoplasm. This will allow a more localized and controlled release of the drug.

■ ASSOCIATED CONTENT

Supporting Information. Part 1, a table summarizing the main structural features of the microbubbles and a schematic representation of MB shell; part 2, a scheme of the chemical structure of the HAox samples; part 3, a scheme of the conjugation of HA with PVA chains onto the shell surface of microbubbles; part 4, a figure with the ^{1}H NMR spectrum of the oxidized hyaluronic acid HAox0.8 with TBC in D_2O; and part 5, a figure with the DOXO release by MCs. This material is available free of charge via the Internet at http://pubs.acs.org.

■ AUTHOR INFORMATION

Corresponding Author

*Fax: +39 06 7259 4328. E-mail: paradossi@stc.uniroma2.it.

■ ACKNOWLEDGMENT

This work was carried out within the frame of the European Project SIGHT "Systems for in-situ theranostics using microparticles triggered by ultra-sound" (www.sight4health.eu) with

the financial support from the European Commission. We kindly acknowledge the National Chemical Laboratories, Pune, India, for the elemental analysis tests and Prof. Federico Bordi, Department of Physics, University of Rome "Sapienza", for the assistance in ζ-potential measurements.

REFERENCES

(1) Lanza, G. M.; Wickline, S. A. *Curr. Probl. Cardiol.* **2003**, *28*, 625–653.
(2) Unger, E. C.; Hersh, E.; Vannan, M.; Matsunaga, T. O.; McCreery, T. *Prog. Cardiovasc. Dis.* **2001**, *44*, 45–54.
(3) Pysz, M. A.; Gambhir, S. S.; Willmann, J. K. *Clin. Radiol.* **2010**, *65*, 500–516.
(4) Willmann, J. K.; Paulmurugan, R.; Chen, K.; Gheysens, O.; Rodriguez-Porcel, M.; Lutz, A. M.; Chen, I. Y.; Chen, X.; Gambhir, S. S. *Radiology* **2008**, *246* (2), 508–518.
(5) Barreiro, O.; Aguilar, R. J.; Tejera, E.; Megías, D.; de Torres-Alba, F.; Evangelista, A.; Sánchez-Madrid, F. *JACC Cardiovasc. Imaging* **2009**, *2* (8), 997–1005.
(6) Reinhardt, M.; Hauff, P.; Linker, R. A.; Briel, A.; Gold, R.; Rieckmann, P.; Becker, G.; Toyka, K. V.; Mäurer, M.; Schirner, M. *Neuroimage* **2005**, *27* (2), 267–268.
(7) Weller, G. E. R.; Lu, E.; Csikari, M. M.; Klibanov, A. L.; Fischer, D.; Wagner, W. R.; Villanueva, F. S. *Circulation* **2003**, *108* (2), 218–224.
(8) Willmann, J. K.; Kimura, R. H.; Deshpande, N.; Lutz, A. M.; Cochran, J. R.; Gambhir, S. S. *J. Nucl. Med.* **2010**, *51* (3), 433–440.
(9) Pysz, M. A.; Foygel, K.; Rosenberg, J.; Gambhir, S. S.; Schneider, M.; Willmann, J. K *Radiology* **2010**, *256*, 519–527.
(10) Garg, H. G.; Hales, C. A. *Chemistry and Biology of Hyaluronan*, 1st ed.; Elsevier: Oxford, 2004.
(11) Underhill, C. B.; Thurn, A. L.; Lacy, B. E. *J. Biol. Chem.* **1985**, *260*, 8128–33.
(12) Underhill, C. B.; Green, S. J.; Comoglio, P. M.; Tarone, G. *J. Biol. Chem.* **1987**, *26*, 13142–46.
(13) Turley, E. A.; Austen, L.; Vandeligt, K.; Clary, C. *J. Cell. Biol.* **1991**, *112*, 1041–47.
(14) McCourt, P. A.; Ek, B.; Forsberg, N.; Gustafson, S. *J. Biol. Chem.* **1994**, *269*, 30081–30084.
(15) Comper, W. D. Molecular Components and Interactions. *Extracellular Matrix*; Harwood Academic Publishers: Amsterdam, 1996; Vol. 2.
(16) Aruffo, A.; Stamenkovic, I.; Melnick, M.; Underhill, C. B.; Seed, B. *Cell* **1990**, *61*, 1303–1313.
(17) Ponta, H.; Sherman, L.; Herrlich, P. A. *Nat. Rev. Mol. Cell. Biol.* **2003**, *4*, 33–45.
(18) Siegelman, M. H.; DeGrendele, H. C.; Estess, P. *J. Leukocyte Biol.* **1999**, *66*, 315–321.
(19) Fernández, J. C.; Vizoso, F. J.; Corte, M. D.; Gava, R. R.; Corte, M. G.; Suárez, J. P.; García-Muñíz, J. L.; García-Morán, M. *Cancer Invest.* **2004**, *22*, 878–885.
(20) Tanabe, K. K.; Ellis, L. M.; Saya, H. *Lancet* **1993**, *341*, 725–726.
(21) Mulder, J. W.; Kruyt, P. M.; Sewnath, M.; Oosting, J.; Seldenrijk, C. A.; Weidema, W. F.; Offerhaus, G. J.; Pals, S. T. *Lancet* **1994**, *344*, 1470–2.
(22) Shutt, E. G.; Klein, D. H.; Mattrey, R .M.; Riess, J. G. *Angew. Chem., Int. Ed.* **2003**, *42*, 3218–35.
(23) Feinstein, S. B. *Am. J. Physiol. Heart Circ. Physiol.* **2004**, *287*, H450–7.
(24) Cavalieri, F.; El Hamassi, A.; Chiessi, E.; Paradossi, G. *Langmuir* **2005**, *21*, 8758–64.
(25) DeMerlis, C. C.; Schoneker, D. R. *Food Chem. Toxicol.* **2003**, *41*, 319–26.
(26) Kobayashi, M.; Toguchida, J.; Oka, M. *Biomaterials* **2003**, *24*, 639–47.
(27) Paradossi, G.; Cavalieri, F.; Chiessi, E. *J. Mater. Sci: Mater. Med.* **2003**, *14*, 687–691.
(28) Cavalieri, F.; El Hamassi, A.; Chiessi, E.; Paradossi, G.; Villa, R.; Zaffaroni, N. *Biomacromolecules* **2006**, *7*, 604–611.
(29) Tortora, M.; Oddo, L.; Margheritelli, S.; Paradossi, G. In *Ultrasound Contrast Agents*; Paradossi, G., Pellegretti, P., Trucco, A., Eds.; Springer-Verlag: Milan, 2010; pp 25−39.
(30) Cavalieri, F.; Finelli, I.; Tortora, M.; Mozetic, P.; Chiessi, E.; Polizio, F.; Brismar, T. B.; Paradossi, G. *Chem. Mater.* **2008**, *20*, 3254–3258.
(31) Jia, X. Q.; Burdick, J. A.; Kobler, J.; Clifton, R. J.; Rosowski, J. J.; Zeitels, S. M.; Langer, R. *Macromolecules* **2004**, *37*, 3239–3248.
(32) Mosman, T. *J. Immunol. Methods* **1983**, *65*, 55–63.
(33) Grishenkov, D.; Pecorari, C.; Brismar, T. B.; Paradossi, G. *Ultrasound Med. Biol.* **2009**, *35*, 1127–1138.
(34) Grishenkov, D.; Pecorari, C.; Brismar, T. B.; Paradossi, G. *Ultrasound Med. Biol.* **2009**, *35*, 1139–1147.
(35) Mercuri, J. J.; Lovekamp, J. J.; Simionescu, D. T.; Vyavahare, N. R. *Biomaterials* **2007**, *28*, 496–503.
(36) Lovekamp, J.; Vyavahare, N. *J. Biomed. Mater. Res.* **2001**, *56*, 478–86.
(37) Varghese, O. P.; Sun, W.; Hilborn, J.; Ossipov, D. *J. Am. Chem. Soc.* **2009**, *131*, 8781–83.
(38) Painter, T.; Larsen, B. *Acta Chem. Scand.* **1970**, *24*, 813–33.
(39) Buffington, L. A.; Pysh, E. S.; Chakrabarti, B.; Balazs, E. A. *J. Am. Chem. Soc.* **1977**, *99*, 1730–34.
(40) Cantor, C. R.; Schimmel, P. R. *Biophysical Chemistry*; Freeman and Company: San Francisco, 1980; Vol. II.
(41) Fernandez, P.; Pretzl, M.; Fery, A.; Tzvetkov, G.; Fink, R. In *Ultrasound Contrast Agents*; Paradossi, G., Pellegretti, P., Trucco, A., Eds.; Springer-Verlag: Milan, 2010; pp 109−127.
(42) Balaban, N. Q.; Schwarz, U. S.; Riveline, D.; Goichberg, P.; Tzur, G.; Sabanay, I.; Mahalu, D.; Safran, S.; Bershadsky, A.; Addadi, L.; Geiger, B. *Nat. Cell Biol.* **2001**, *3*, 466–472.
(43) Muñoz, J. A.; Kreft, O.; Semmling, M.; Kempter, S.; Skirtach, A. G.; Bruns, O. T.; del Pino, P.; Bedard, M. F.; Rädler, J.; Käs, J.; Plank, C.; Sukhorukov, G. B.; Parak, W. J. *Adv. Mater.* **2008**, *20*, 4281–87.
(44) Conner, S. D.; Schmid, S. L. *Nature* **2003**, *422*, 37–44.
(45) Sukhorukov, G. B.; Rogach, A. L.; Zebli, B.; Liedl, T.; Skirtach, A. G.; Köhler, K.; Antipov, A. A.; Gaponik, N.; Susha, A. S.; Winterhalter, M.; Parak, W. J. *Small* **2005**, *1*, 194–200.
(46) Munõz, J. A.; Kreft, O.; Alberola, A. P.; Kirchner, C.; Zebli, B.; Susha, A. S.; Horn, E.; Kempter, S.; Skirtach, A. G.; Rogach, A. L.; Rädler, J.; Sukhorukov, G. B.; Benoit, M.; Parak, W. J. *Small* **2006**, *2*, 394–400.
(47) De Geest, B. G.; Vandenbroucke, R. E.; Guenther, A. M.; Sukhorukov, G. B.; Hennink, W. E.; Sanders, N. N.; Demeester, J.; De Smedt, S. C. *Adv. Mater.* **2006**, *18*, 1005–1009.
(48) Reibetanz, U.; Claus, C.; Typlt, E.; Hofmann, J.; Donath, E. *Macromol Biosci.* **2006**, *6*, 153–160.
(49) Semmling, M.; Kreft, O.; Muñoz, J. A.; Sukhorukov, G. B.; Käs, J.; Parak, W. J. *Small* **2008**, *4*, 1763–1768.
(50) De Geest, B. G.; De Koker, S.; Sukhorukov, G. B.; Kreft, O.; Parak, W. J.; Skirtach, A. G.; Demeester, J.; De Smedt, S. C.; Hennink, W. E. *Soft Matter* **2009**, *5*, 282–291.
(51) Javier, A. M.; Kreft, O.; Semmling, M.; Kempter, S.; Skirtach, A. G.; Bruns, O. T.; Pino, P.; Bedard, M. F.; Rädler, J.; Plank, C.; Sukhorukov, G. B.; Parak, W. J. *Adv. Mater.* **2008**, *20*, 4281–4287.
(52) Manocha, B.; Margaritis, A. *J. Nanomater.* **2010**, doi: 10.1155/2010/780171.
(53) Liu, J.; Jiang, X.; Ashley, C.; Brinker, C. J. *J. Am. Chem. Soc.* **2009**, *131* (22), 7567–7569.
(54) Nasongkla, N.; Bey, E.; Ren, J.; Ai, H.; Khemtong, C.; Guthi, J. S.; Chin, S.; Sherry, D. A.; Boothman, D. A.; Gao, J. *Nano Lett.* **2006** *6* (11), 2427–2430.
(55) Felgner, P. L.; Gadek, T. R.; Holm, M.; Roman, R.; Chan, H. W.; Wenz, M.; Northrop, J. P.; Ringold, G. M.; Danielsen, M. *Proc. Natl. Acad. Sci. U.S.A.* **1987**, *84*, 7413–7417.
(56) Felgner, P. L. *Sci. Am.* **1997**, *276*, 102–106.
(57) Caracciolo, G.; Pozzi, D.; Amenitsch, H.; Caminiti, R. *Langmuir* **2005**, *21*, 11582–11587.